Applied Nanoscience (2024) 14:997–1012
https://doi.org/10.1007/s13204-024-03062-x

ORIGINAL ARTICLE

Investigating electrocatalytic properties of β_{12}-borophene as a cathode material for an efficient lithium-oxygen battery: a first-principles study

C. Fwalo[1,2] · A. Kochaev[3] · R. E. Mapasha[1]

Received: 17 May 2024 / Accepted: 18 July 2024 / Published online: 1 August 2024

Abstract

Responding to the pressing need to mitigate climate change effects due to fossil fuel consumption, there is a collective push to transition towards renewable and clean energy sources. However, the effectiveness of this move depends on an efficient energy storage system that surpasses current lithium-ion battery technology. The lithium-oxygen battery, having significantly high theoretical specific capacity compared to other systems, has emerged as a promising solution. However, the issues of poor cathode electrode conductivity and slow kinetics during discharge product formation have limited its practical applications. In this work, the first principles-based density functional theory was used to investigate the electrocatalytic properties of β_{12}-borophene as a cathode electrode material for a high-performance lithium-oxygen battery. The adsorption energy, charge density distributions, Gibbs free energy changes, and diffusion energy barriers of lithium superoxide (LiO_2) on β_{12}-borophene were calculated. Our findings revealed several important insights: The adsorption energy was found to be − 3.70 eV, suggesting a strong tendency for the LiO_2 to remain anchored to the material during the discharging process. The dynamics in the charge density distributions between LiO_2 and the β_{12}-borophene substrate exhibited complex behavior. The analysis of the Gibbs free energy changes of the reactions yielded an overpotential of − 1.87 V, this moderate value suggests spontaneous reactions during the formation of the discharge products. Most interestingly, the density of states and band structure analysis suggested the preservation of metallic properties and improved electrical conductivity of the material after the adsorption of LiO_2. Additionally, β_{12}-borophene has a relatively low diffusion energy barrier of 1.08 eV, implying effortless diffusion of the LiO_2 and an increase in the rate of discharging process. Ultimately, the predicted electronic properties of β_{12}-borophene, make it a strong candidate as a cathode electrode material for an efficient lithium-oxygen battery.

Keywords Lithium-superoxide · β_{12}-borophene · Density functional theory · Charge density distributions · Gibbs free energy · Diffusion energy barrier

Abbreviations

DFT	Density functional theory
LIO_2	Lithium superoxide
LI_2O_2	Lithium peroxide
O_2	Oxygen molecule
Li	Lithium ion
NEB	Nudged elastic band
β_{12}	Beta-12
TDOS	Total density of states
PDOS	Projected density of states
ORR	Oxidation–reduction reaction

✉ C. Fwalo
fwalochewe99@gmail.com

[1] Department of Physics, University of Pretoria, Pretoria, South Africa

[2] Department of Physics, Copperbelt University, Kitwe, Zambia

[3] Research and Education Center "Silicon and Carbon Nanotechnologies", Ulyanovsk State University, Ulyanovsk, Russia

Introduction

Climate change poses a significant threat to the world today, with fossil fuel emissions identified as the primary contributor (Höök and Tang 2013). To significantly reduce these emissions such as carbon dioxide, societies must transition from fossil fuels to clean energy sources (Aurbach et al. 2016). Clean energy can be utilized directly or stored in

energy storage systems like lithium-ion batteries. The lithium-ion batteries are the most prevalent energy storage solution currently due to their high energy density (Placke et al. 2017). They are instrumental in various modern technologies, including electric vehicles (Berckmans et al. 2017), electronic devices (Kamat 2019), and advanced military systems (Mamun et al. 2018). However, technological advancements have brought about limitations in these systems. Thus, there is a pressing need to develop energy storage systems with ultra-high specific capacities, power, and energy densities, to meet the growing energy demands. This necessitates exploring post-lithium-ion battery technologies such as the lithium-oxygen ($Li-O_2$) battery, which is considered an attractive alternative due to its high theoretical specific capacity (Bruce et al. 2012).

Regardless of having high theoretical specific capacity, practical developments in $Li-O_2$ battery technology continue to encounter significant issues, such as inadequate electronic conductivity of the cathode electrode and slow kinetics during the formation and dissociation of discharge products (Liu et al. 2020; Tan et al. 2017). These challenges are attributed to the insulation of the formed lithium superoxide (LiO_2), serving as the intermediate discharge product(Halder et al. 2018; Lu et al. 2016), and the choice of material for the cathode electrode (Tan et al. 2017). As a result, researchers are focused on exploring materials that could effectively serve as cathode electrodes to overcome the reported issues. In this regard, 2D materials are being explored as the prime candidate for the challenges. These materials have garnered significant attention due to their unique properties, such as a large surface area, and favorable electronic and chemical attributes. Notably, graphene has been extensively investigated among these 2D materials (Avouris and Dimitrakopoulos 2012; Choi et al. 2010). For instance, research efforts have delved into understanding the adsorption mechanisms of lithium oxides (Li_xO_2) on graphene to gain insights into oxidation–reduction reactions (ORRs) and oxygen evolution reactions (OERs) (Karimzadeh et al. 2023). Findings revealed the spontaneous adsorption of Li, O_2, LiO_2, and Li_2O_2 species on graphene, signifying its potential as a cathode electrode material. Moreover, doping graphene with nitrogen (N) atoms has shown improved adsorption and preserved metallic characteristics after species absorption (Karimzadeh et al. 2023). Furthermore, reports indicate that graphene doped with boron can potentially enhance ORRs and OERs in the context of $Li-O_2$ batteries (Jiang et al. 2016).

After significant research into the exceptional properties of graphene (Avouris and Dimitrakopoulos 2012; Choi et al. 2010), it has been discovered that various other 2D materials, such as silicene (Yu 2019), MnO_2 nanorods (Geaney and O'Dwyer 2015), $2D-Nb_2O_5$ (Li and Yu 2021b), doped boron nitride surfaces (Chowdhury and Datta, 2018), single-layer Tl_2O (Li et al. 2020b), germanium monochalcogenides (Ji et al. 2017), $2D-MoO_3$ (Li et al. 2021), siligraphanes (Dong et al. 2018), and the pillared $\delta-MnO_2$ with spaces enlarged (Li and Yu 2021a), exhibit potential properties as cathode electrode materials. These materials have shown promise in catalyzing electrochemical reactions and could pave the way for the practical realization of a $Li-O_2$-battery.

Additionally, borophenes consisting of boron elements, are among the 2D materials that have also received significant attention due to their similarity to graphene in terms of chemistry. This is due to their proximity in the periodic table (Scerri 2019; Jemmis and Jayasree 2003). Most interestingly about these materials, is that their theoretical specific capacities exceed that of graphene due to the lighter atomic weight of boron element (Wieser and Coplen 2010). Recently, various 2D boron polymorphs, including β_{12}-borophene, have been successfully exfoliated and synthesized on Ag (111) substrates using different techniques (Mannix et al. 2015; Rubab et al. 2020; Feng et al. 2016b). β_{12}-borophene exhibits unique properties such as high electronic conductivity, large surface area (Feng et al. 2016b, a), and strong mechanical properties (Peng et al. 2017), making it suitable for numerous potential applications in various fields. Due to these distinctive properties, β_{12}-borophene has garnered significant attention from scientists and engineers. Its tailored properties and potential applications in electronic devices are currently under investigation. For instance, its electronic transport alterations under strain and electric fields are being studied (Davoudiniya and Mirabbaszadeh 2021). Furthermore, the electronic-optical properties of β_{12}-borophene change with adsorbed gas molecules (Hieu et al. 2023), as well as changes in its electronic and thermal properties due to substrate-induced strain and exchange fields (Hoi et al. 2024). Moreover, β_{12}-borophene has shown potential in areas such as gas sensing for toxic gases (Yu et al. 2020), as an anode material in lithium and sodium ion batteries (Karimzadeh et al. 2023; Zhang et al. 2016; Mortazavi et al. 2017), and as a cathode electrode material in lithium-sulfur and oxygen batteries (Rao et al. 2019; Jiang et al. 2018; Fwalo et al. 2024).

Although numerous reports about the properties and potential applications of β_{12}-borophene as a cathode electrode material in lithium-sulfur batteries, there is limited and unclear information available concerning the adsorption mechanisms of lithium superoxide (LiO_2) as an intermediate discharge product and its impact on β_{12}-borophene as a cathode electrode material in lithium-oxygen batteries, particularly regarding charge density distributions, diffusion, and electronic conductivity. In this study, the first principles-based density functional theory (DFT) was utilized to investigate the adsorption, diffusion mechanisms, and electronic properties of β_{12}-borophene adsorbed with LiO_2. To

achieve this: Firstly, the crystal structure of β_{12}-borophene was created and the configurations of lithium-ion (Li), oxygen molecule (O_2), and LiO_2 at various potential adsorption sites within the unit cell of β_{12}-borophene were created. Subsequently, the most energetically stable configurations by computing the adsorption energies were determined. Finally, characterization of electronic properties was done, including charge density difference distributions, Gibbs free energy changes, the density of states (DOS), band structures, and diffusion energy barriers. Based on the results obtained, the prospect of the β_{12}-borophene as a cathode material in the lithium-oxygen battery was assessed.

Computational methods

In this work, all density functional theory (DFT) related calculations were performed using the quantum ESPRESSO code (Giannozzi et al. 2017, 2009). The exchange and correlation energy of interacting electrons were treated using generalized gradient approximation (GGA) within the function of Perdew-Burke-Ernzerhof (PBE) (Grimme 2006; Stampfl et al. 2001; Perdew et al. 1998; Ernzerhof and Scuseria 1999). To describe the core electrons of the crystal structure, a projector-augmented wave (PAW) potential was employed (Blöchl 1994). After tests of convergence, a kinetic energy cut-off of 680 eV was adopted, and using the Monkhorst–Pack scheme within the Brillouin zone (Monkhorst and Pack 1976; Chadi 1977) a K-points sampling of $13\times9\times1$ was used. Within an energy difference of 10^{-5} eV, and Hellman–Feynman force convergence of 10^{-6} eV/Å, a fully relaxed β_{12}-borophene crystal was achieved until all the atomic positions had converged. Methfessel and Paxton (MP) occupational function was used to smear electrons (Methfessel and Paxton 1989). DFT-D3 correction with the Grimme Scheme was employed to correct the effects of van der Waals forces due to the introduction of species on the crystal structure (Ehrlich et al. 2011). To account for the possible effects of magnetism due to the introduced foreign species on the substrate, spin-orbital coupling was incorporated into all the calculations. A vacuum space of 15 Å in the c-direction was used to avoid the effects of periodic

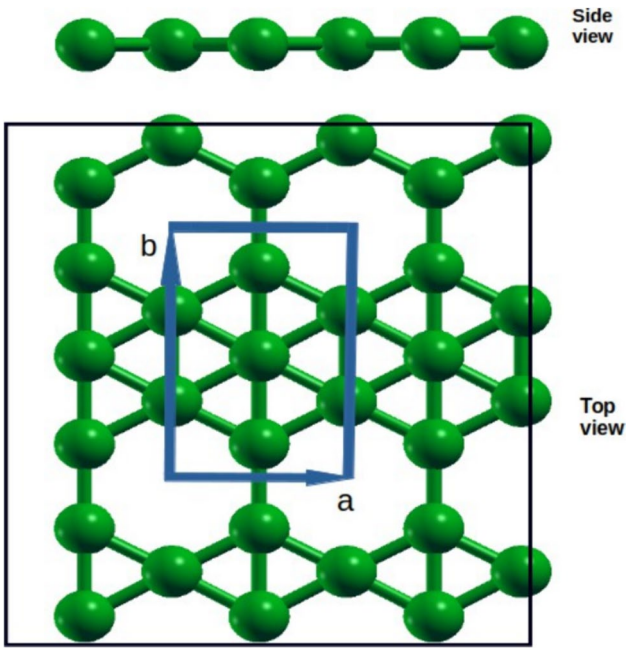

Fig. 1 Top and side views of the crystal structure: A primitive unit cell enclosed in a blue rectangle consisting of 5 boron atoms and a single vacancy. All boron atoms are represented by the color green. Additionally, **a** and **b** are the lattice parameters

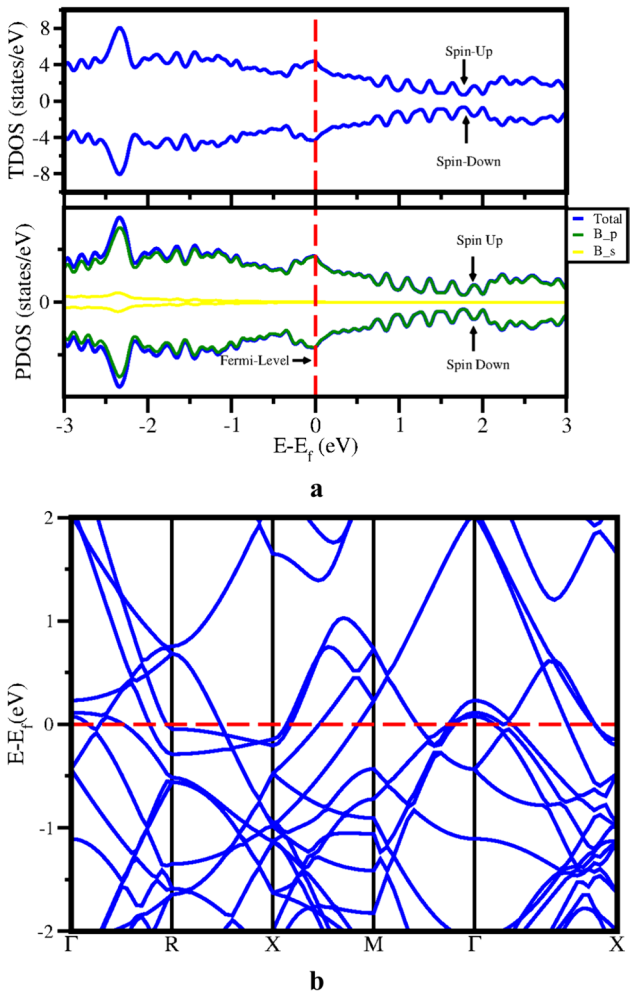

Fig. 2 Density of states (DOS) and bands structure of pristine β_{12}-borophene: **a** Total density of states (TDOS) and projected density of states (PDOS), **b** bands structure of β_{12}-borophene. The dashed red line denotes the Fermi level

images of crystal structures. To increase adsorption sites and avoid interactions between the species within the adjacent adsorption sites, a supercell of $3\times2\times1$ (30 boron atoms) was created using VESTA (Momma and Izumi 2008). To calculate the adsorption energies of the species adsorbed on the crystal surface, the following equation was used:

$$E_{ads} = \left(E_{system} - E_{pristine} - n * E_{species}\right)/n \quad (1)$$

Here, E_{system} denotes total energy for the β_{12}-borophene adsorbed with species, $E_{pristine}$ is the total energy for pristine β_{12}-borophene, $E_{species}$ is the total energy for the free species (in a vacuum), and n denotes the total number of species adsorbed by the substrate. To have a better understanding of the charge interactions between species- and the substrate, a topological analysis of the electric charge density was performed. This was achieved by calculating the charge density difference distributions using the following equation:

$$\rho_{charge} = \rho_{system} - \rho_{substrate} - \rho_{species} \quad (2)$$

where ρ_{charge} denotes the charge density difference between the substrate and adsorbate in the vacuum,

ρ_{system} denotes the complex system charge density (substrate with the species), $\rho_{substrate}$ represents the density of charge of the substrate without a species, and $\rho_{species}$ signifies the charge density of the species in a vacuum. It should be noted that the atomic positions of the substrate without a species, and the species in a vacuum are maintained as in the species on substrate system (Neugebauer and Scheffler 1992).

To determine the spontaneity of the reactions on β_{12}-borophene during the formation of the intermediate discharge product of LiO_2, the change in Gibbs free energies (ΔG) for the reactions was calculated. However, before that, the chemical potential (CP) for each species involved in the ORRs was calculated using the following equation (Xu et al. 2018):

$$CP = E_{DFT}(species) + ZPE(species) - TS \quad (3)$$

Here, E_{DFT}(species) denotes the total energy of the optimized system for Li, O_2, and LiO_2 adsorbed on β_{12}-borophene. The ZPE (species) denotes the zero point energy of the molecular species, calculated by summing all the normal vibrational frequencies. Since all our calculations were performed at 0 K, the entropy contributions from all the species were ignored (TS = 0). After increasing the concentration of the LiO_2 on the β_{12}-borophene, the potentials were calculated using the following equation (Xu et al. 2018)

$$V = \left(-\left|\Delta G\left(LiO_2\right)\right|\right)/e \quad (4)$$

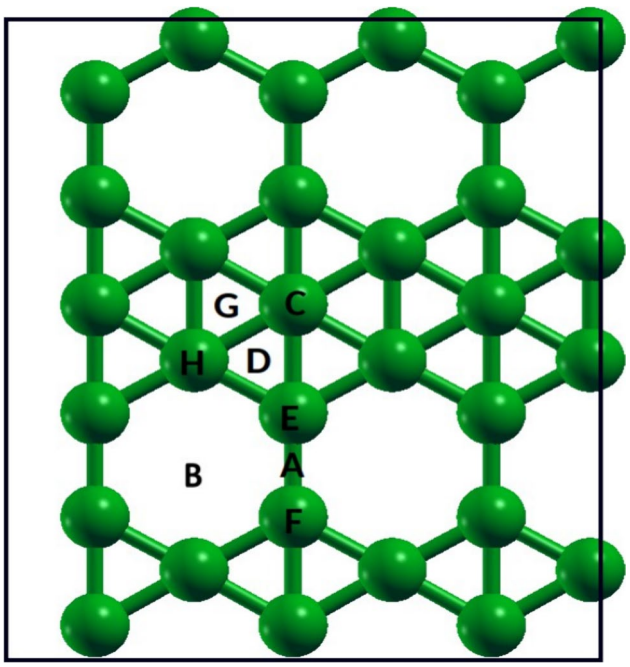

Fig. 3 Possible identified adsorption sites within the unit cell: A, B, C, D, E, F, G, and H sites

Results and discussion

Optimized crystal structure and metallic characteristics of pristine β_{12}-borophene

The crystal structure of β_{12}-borophene was created based on the Pmm2 space group and an orthorhombic crystal system (Marder 2010). The optimized structure revealed a rectangular primitive unit cell containing 5 boron atoms with a single vacancy, and it had lattice parameters of $a = 2.925$ Å and $b = 5.093$ Å. The borophene structure comprises a chain of hollow hexagons and a chain of hexagonal boron atoms, and it appears flat without any corrugations (Fig. 1). These lattice parameters are very close to what was obtained in previous first-principles studies (Zhang et al. 2016; Grixti et al. 2018; Karimzadeh et al. 2023; He et al. 2020), with very minimal discrepancies due to different conditions set for the simulations.

Furthermore, the dynamical and thermodynamical stabilities of the β_{12}-borophene crystal were assessed before it could be used for further electronic properties predictions: For thermodynamical stability, the cohesive energy (E_{coh}) (Sun et al. 2017) was calculated using the equation:

$$E_{coh} = E_{bulk} - n * E_{iso} \quad (5)$$

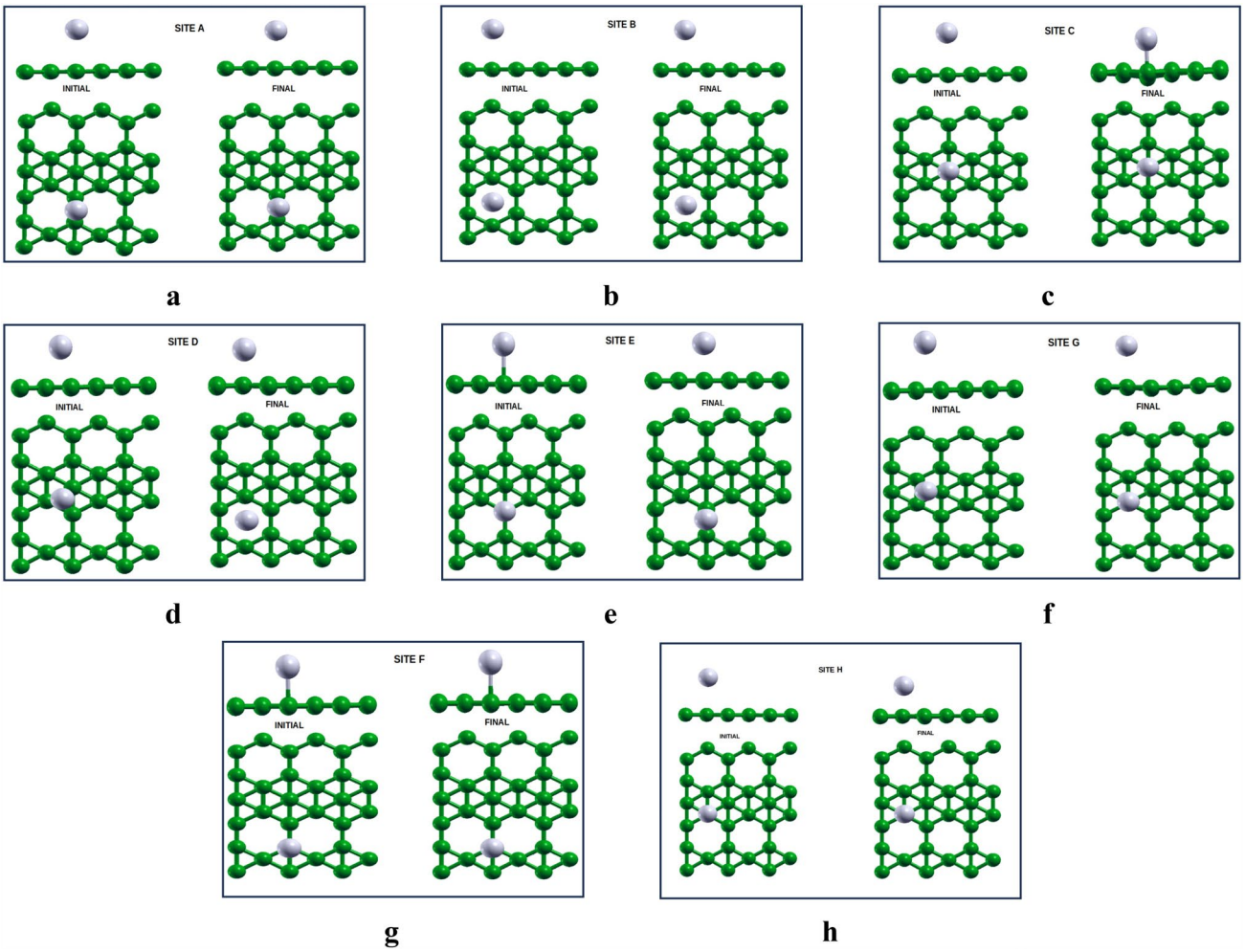

Fig. 4 Initial (left) and final (right) configurations of Li on β_{12}-borophene: **a** side and plan views of SITE A, **b** side and top views of SITE B, **c** side and top views of SITE C, **d** side and top views of SITE D, **e** side and top views of SITE E, **f** side and top views of SITE F, **g** side and top views of SITE G, and **h** side and top views of SITE H. The lithium and boron atoms are represented by the colors grey and green, respectively

Table 1 The calculated properties of optimized configurations of Li at different sites of β_{12}-borophene: Adsorption sites, adsorption energies and binding distances

Adsorption Site	Adsorption Energy (eV)	Binding Distance (Å)
Site A	− 1.27	2.59
Site B	− 2.24	2.00
Site C	− 1.54	2.19
Site D	− 1.88	2.06
Site E	− 1.80	2.09
Site F	− 1.63	2.21
Site G	− 1.49	2.20
Site H	− 1.57	2.18

where E_{bulk} represents the total energy for the primitive unit cell, n denotes the total number of atoms in a unit cell, and E_{iso} indicates the total energy for an isolated boron atom. The calculated cohesive energy for β_{12}-borophene was 5.64 eV/atom. Notably, this value aligns with previous reports where cohesive energies of 6.147 eV (Peng et al. 2017) and 5.71 eV (Sun et al. 2017) were observed. The cohesive value obtained shows that β_{12}-borophene is stable thermodynamically. The effects of dynamics and temperature on the structure's stability have been explored elsewhere, where the phonon dispersion spectrum was calculated, and the analysis revealed no negative frequencies. Moreover, for thermal stability, ab initio molecular dynamics (AIMD) was utilized to analyze structural distortion at extreme temperatures, indicating that β_{12}-borophene is dynamically and thermodynamically stable (Peng et al. 2017; Mortazavi et al. 2017).

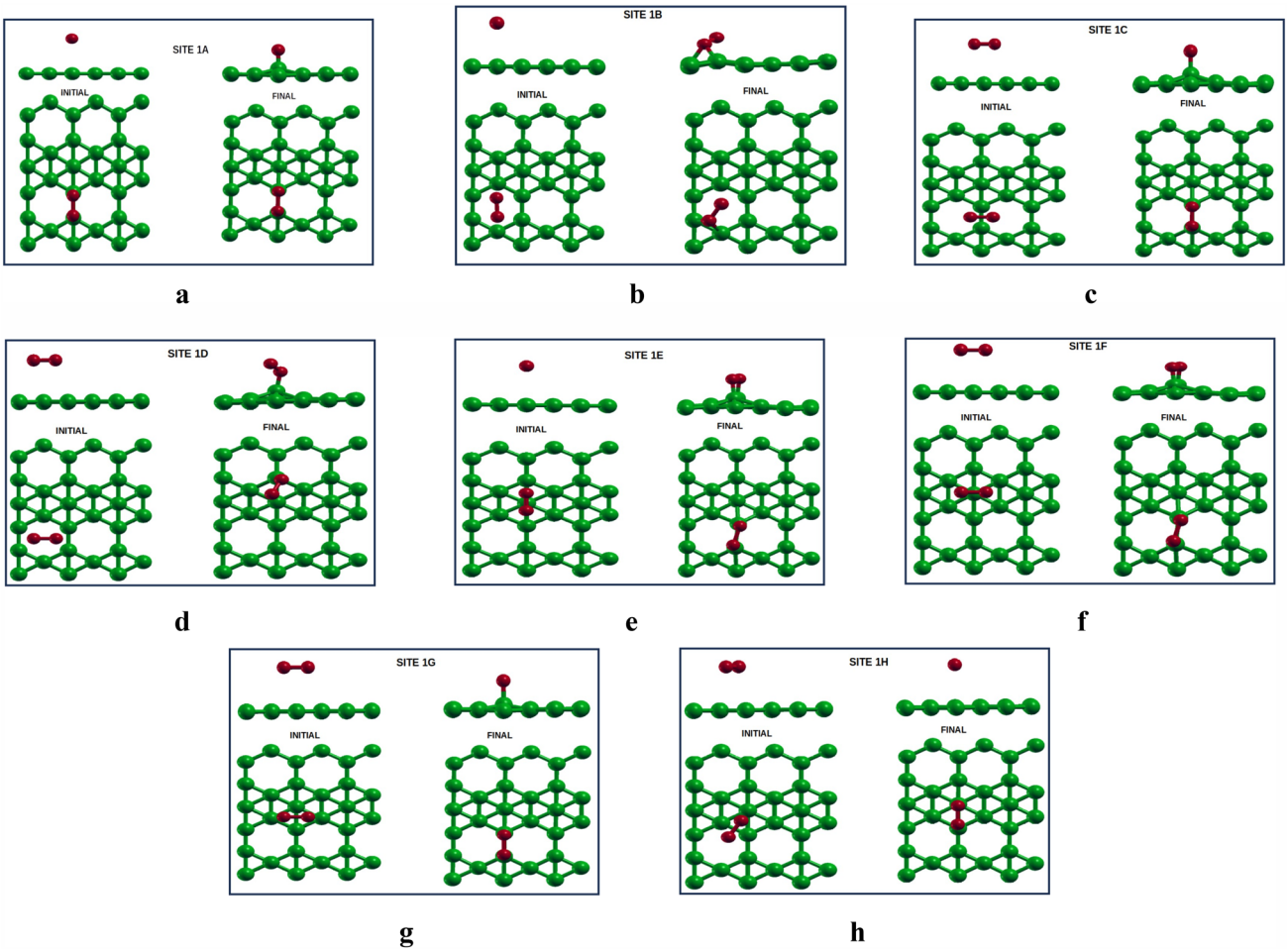

Fig. 5 Initial (left) and final (right) configurations of O_2 on β_{12}-borophene: **a** side and top views of SITE 1A, **b** side and top views of SITE 1B, **c** side and top views of SITE 1C, **d** side and top views of SITE 1D, **e** side and top views of SITE 1E, **f** side and top views of SITE 1F, **g** side and top views of SITE 1G, and **h** side and top views of SITE 1H. The oxygen and boron atoms are represented by colors red and green, respectively

After evaluating the stability of β_{12}-borophene, its electronic properties in its pure form were investigated by calculating the total density of states (TDOS), the projected density of states (PDOS), and bands structure (Fig. 2). The findings revealed that it exhibits metallic properties, as evidenced by overlapping conduction and valence bands, indicating a zero band gap along the Fermi level. The primary orbitals along the Fermi level were identified as the boron atom 2p-orbitals, with minimal contributions from s-orbitals. These outcomes are in line with previously reported studies (Luo et al. 2017; Feng et al. 2016b; Li et al. 2020a; Grixti et al. 2018) where it was observed that the valency and conduction bands overlap with a high concentration of electronic states along the Fermi level. This indicates the excellent metallic characteristics of the β_{12}-borophene and lays the groundwork for further exploration of its electronic properties following the adsorption of other species.

Table 2 The calculated properties of optimized O_2 configurations at different sites of β_{12}-borophene; adsorption energies, binding distances and O_2 bond lengths

Adsorption Site	Adsorption Energy (eV)	Binding Distance (Å)	O_2 bond length (Å)
Site 1A	− 5.15	1.69	1.46
Site 1B	− 3.93	1.88	1.36
Site 1C	− 2.96	2.13	1.43
Site 1D	− 4.09	2.51	1.33
Site 1E	− 1.80	2.20	1.29
Site 1F	− 5.13	1.60	1.45
Site 1G	− 4.99	1.83	1.43
Site 1H	− 3.72	2.75	1.33

Species configurations on β_{12}-borophene

During the discharging process, lithium atoms are oxidized and diffuse to the cathode electrode via the electrolyte. Upon reaching the surface of the cathode electrode, they combine with O_2 from the ambient environment to form LiO_2 in the presence of electrons, a reaction mechanism known as the oxygen reaction reduction (ORR) (Bruce et al. 2012; Aurbach et al. 2016). As part of this mechanism, the formed LiO_2 is adsorbed at the surface of the cathode electrode, giving rise to numerous possible configurations and orientations. Bearing this in mind, different potential adsorption sites were identified and labeled as sites A to H within the supercell (Fig. 3).

Lithium-ion (Li) on β_{12}-borophene

As previously mentioned, the formation of LiO_2 involves the combination of Li and O_2. Consequently, configurations of all the species of interest were introduced on the surface of the crystal structure. Initially, the focus was on Li by positioning it at different sites (Fig. 3). Eight adsorption sites were considered and labeled as follows: (a) SITE A: at the top of the bridge between hollow hexagons, (b) SITE B: top of the center of the hollow hexagon, (c) SITE C: top of the boron atom and center of the hexagon, (d) SITE D: top of the triangle of boron atoms, (e) SITE E: top of the boron atom bonded to four borons, (f) SITE F: top of the boron atom part of the bridge between hollow hexagons, (g) SITE G: top of the triangle of boron atoms, and (h) SITE H: top of the boron atom bonded to five borons. As shown in Fig. 4, the configurations in their initial (left) and final (right) stages of relaxation were examined. Following a full system relaxation, it was observed that the positions for configurations at SITE A, SITE B, SITE C, SITE G, and SITE H remained unchanged, while SITE D and SITE F migrated towards SITE A and SITE H. This shifting of configurations suggests that the

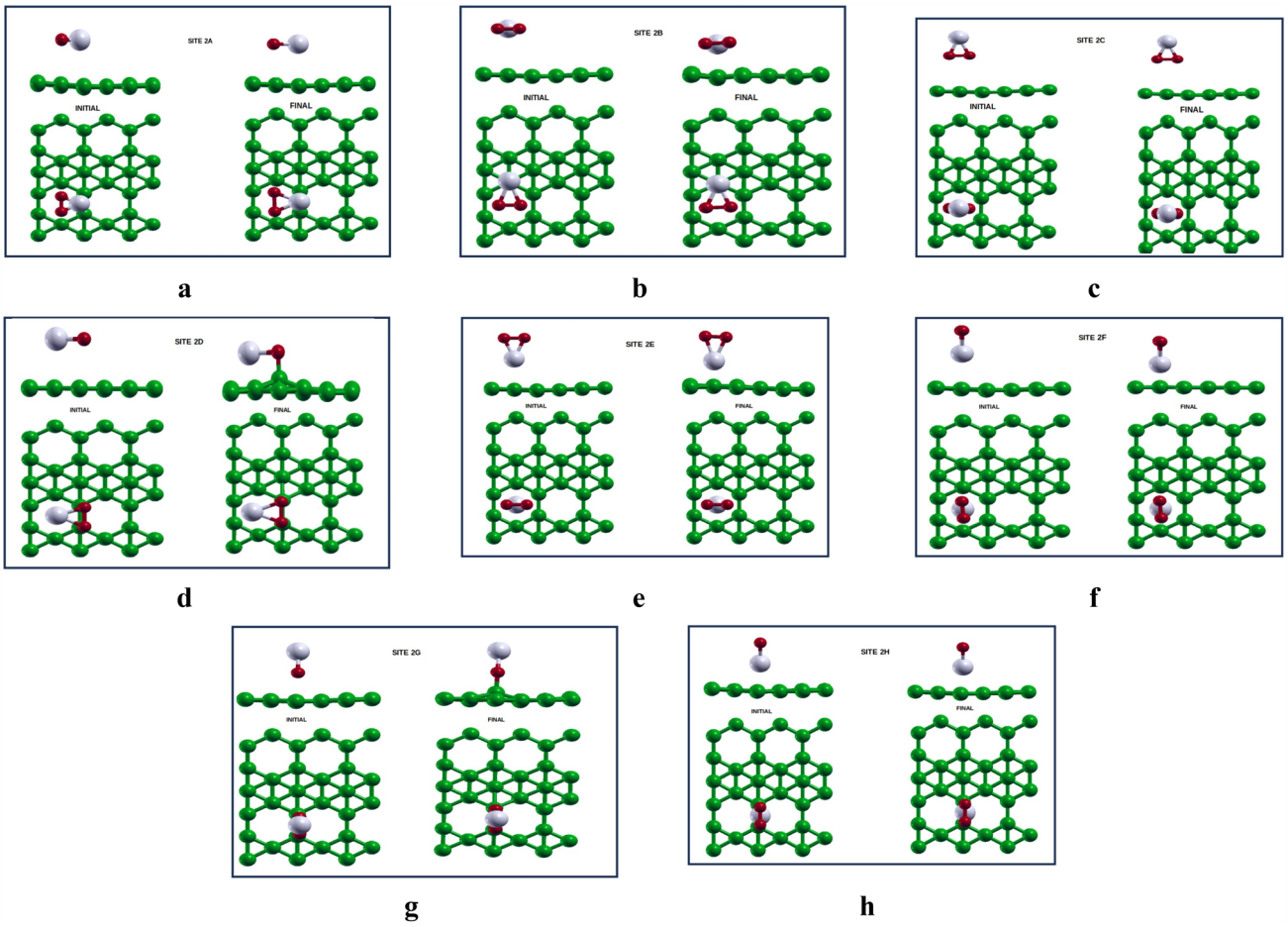

Fig. 6 Initial (left) and final (right) configurations of LiO_2 on β_{12}-borophene: **a** side and top views for SITE 2A, **b** side and top views of SITE 2B, **c** side and top views of SITE 2C, **d** side and top views of SITE 2D, **e** side and top views of SITE 2E, **f** side and top views of SITE 2F, **g** side and top views of SITE 2G, and **h** side and top views of SITE 2H; the lithium, oxygen and boron atoms are represented by color grey, red and green, respectively

Table 3 Relaxed LiO_2 configurations at different sites of β_{12}-borophene: Adsorption sites, adsorption energies and binding distances between Li and O_2 with the surface

Binding distance (Å)			
Adsorption Site	Adsorption Energy (eV)	Li	O_2
Site 2A	− 1.91	2.23	2.37
Site 2B	− 1.80	2.38	2.03
Site 2C	− 0.88	5.21	3.48
Site 2D	− 3.70	2.08	1.54
Site 2E	− 1.84	3.52	1.77
Site 2F	− 1.84	3.62	1.82
Site 2G	− 2.99	1.55	2.27
Site 2H	− 1.53	3.74	2.10

Table 4 Calculated adsorption energy, binding distances, and quantified charge density

Charge Density (e)					
	Adsorption	Binding	Li	O_2	β_{12}-surface
System	Energy (eV)	Distance (Å)			
Li on β_{12}	− 2.24	2.00	+ 0.88	–	− 0.88
O_2 on β_{12}	− 5.15	1.69	–	− 1.98	+ 1.98
LiO_2 on β_{12}	− 3.70	1.79	+ 0.89	− 1.76	+ 0.87

previous sites were not energetically favorable and moved towards the most stable sites.

To have a deeper insight into the adsorption of Li, the adsorption energies were calculated, resulting in values ranging from − 2.24 to − 1.27 eV as detailed in Table 1. Notably, the configuration at SITE B exhibited the highest negative value (− 2.24 eV), suggesting to be the most strongly adsorbed and stable. Furthermore, the calculated binding distances ranged from 2.00 to 2.59 Å (Table 1), with the configuration at SITE B displaying the shortest binding distance (2.00 Å) as depicted in Fig. 4b. This outcome points to a strong interaction with the substrate, aligning with the finding that Li is strongly adsorbed on top of the center of the hollow hexagon of β_{12}-borophene. These results correlate with previously reported DFT work (Karimzadeh et al. 2023; Zhang et al. 2016), where it was found that the Li atom adsorbed on top of the hollow site has the highest adsorption energy. Hence, it is the most stable configuration as compared to others.

Oxygen molecule (O_2) on β_{12}-borophene

As a next step, various configurations for O_2 were explored at different sites and orientations, as illustrated in Fig. 5: (a) SITE 1A: top of the bridge with O_2 axis parallel and its atoms facing boron atoms, (b) SITE 1B: top of the hollow hexagon with O_2 axis facing the boron atoms, (c) SITE 1C: top of the bridge and the molecule axis facing the adjacent hollow hexagons, (d) SITE 1D: top of the hollow hexagon with O_2 axis facing the bridges of a chain of hollow hexagons, (e) SITE 1E: top of the hexagon of boron atoms with molecule axis perpendicular to the chain of hexagons, (f)

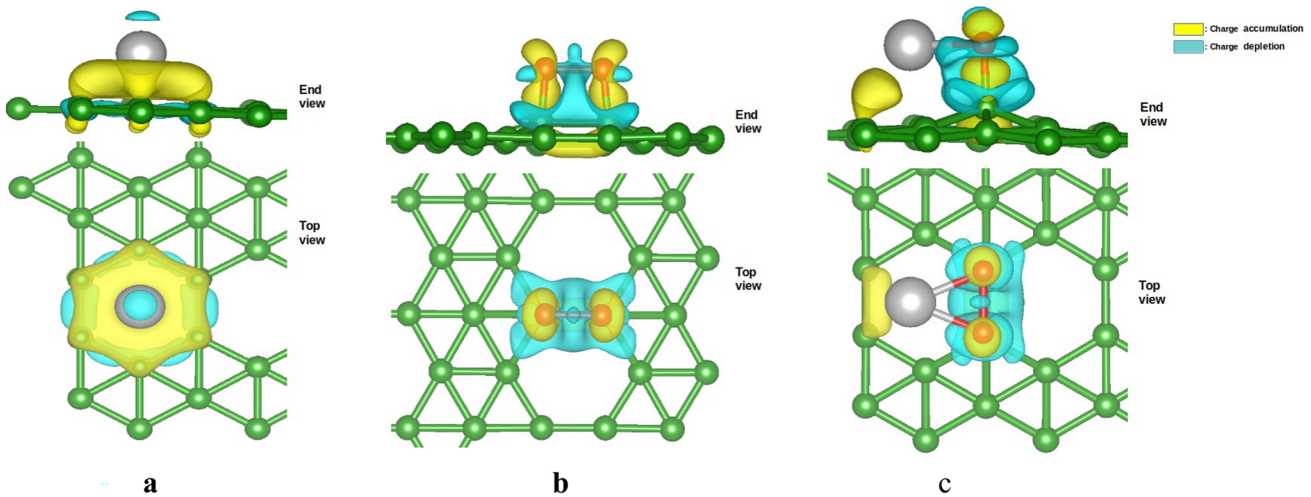

Fig. 7 Charge density difference distribution of adsorbed species on β_{12}-borophene: **a** Li on β_{12}-borophene, **b** O_2 on β_{12}-borophene, and **c** LiO_2 on β_{12}-borophene. The charge depletion and accumulation are represented by blue and yellow colors, respectively

SITE 1F: top of the hexagon of boron atoms with O_2 axis parallel to the chain of hexagons of boron atoms, (g) SITE 1G: O_2 on top of the bond of boron atoms in the hexagon, and (h) SITE 1H: O_2 axis facing the hollow hexagon and hexagon of boron atoms.

After relaxing the systems, it was observed that most of the configurations changed their positions and orientations (Fig. 5). For example, the configuration at SITE 1B (Fig. 5b) diffused towards the edge of a hollow hexagon, with the molecule slanting, indicating instability. Similarly, the configuration at SITE 1D (Fig. 5d) diffused towards the hexagon with boron atoms and also slanted. In contrast, the configuration at SITE 1H (Fig. 5h) migrated towards the hexagon of boron atoms and oriented parallel to the substrate. Except for the configuration at SITE 1A, which maintained its position and orientation, all the other configurations diffused towards SITE 1A. Notably, all the configurations that diffused formed covalent bonds with boron atoms. This formation of covalent bonds between the O_2 and β_{12}-borophene is consistent with previously predicted first-principles results (Luo et al. 2017; Mortazavi et al. 2017). Moreover, the formation of the covalent bonds shows the stability of the systems.

To have further insights into the mechanisms of the configurations, the adsorption energies, bond lengths, and binding distances of O_2 were calculated as detailed in Table 2. The adsorption energies ranged from − 5.15 to − 1.8 eV, with the configuration at SITE 1A exhibiting the most negative adsorption energy (− 5.15 eV), indicative of strong adsorption. Spontaneous adsorption towards oxygen is particularly significant as it allows the material to prevent it from dissociating into the electrolyte and migrating toward the negative electrode (anode), thereby preventing corrosion and potential battery failure. Next, the O_2 bond lengths were calculated and ranged from 1.29 to 1.46 Å. These values were compared to the O_2 in a vacuum (1.20 Å) and the variations indicate the effect of O_2-substrate interactions. Furthermore, the O_2 binding distances were calculated and ranged from 1.69 to 2.75 Å (Table 2), with the configuration at SITE 1A having the shortest distance (1.69 Å). Given its high adsorption energy and the shortest binding distance, the configuration at SITE 1A was considered the most energetically stable configuration compared to the others.

Table 5 The calculated chemical potentials (CPs) for all the species involved in the ORR mechanism; Li, O_2, and pristine β_{12}-borophene and adsorbed LiO_2

System	E_{ZPE} (eV)	CP (eV)
Li	0.0	− 203.33
O_2	0.095	− 910.98
β_{12}	0.0	− 2551
LiO_2*	0.019	− 3669.25

Lithium superoxide (LiO_2) on β_{12}-borophene

For the LiO_2 on β_{12}-borophene system, identifying potential adsorption sites around the vacancy (Fig. 6) were strategically generated. This decision was based on the understanding that the vacancy is the region where the most stable sites for the configurations of LiO_2 (Fig. 4a) and O_2 (Fig. 5d) are located. The identified sites include: (a) Li facing the bridge with O_2 on top of the hollow hexagon with its axis facing boron atoms (SITE 2A), (b) Li positioned on top of the boron atom and O_2 on top of the hollow hexagon (SITE 2B), (c) Li located above O_2, with the O_2 axis facing the bridge (SITE 2C), (d) O_2 positioned on top of the boron atoms at the bridge and Li on top of the hollow hexagon (SITE 2D), (e) Li facing the hollow hexagon with O_2 on top and its axis perpendicular to the bridges of the chain of hollow hexagons (SITE 2E), (f) Li facing the hollow hexagon with the O_2 axis oriented facing the boron atoms (SITE 2F), (g) O_2 on top of

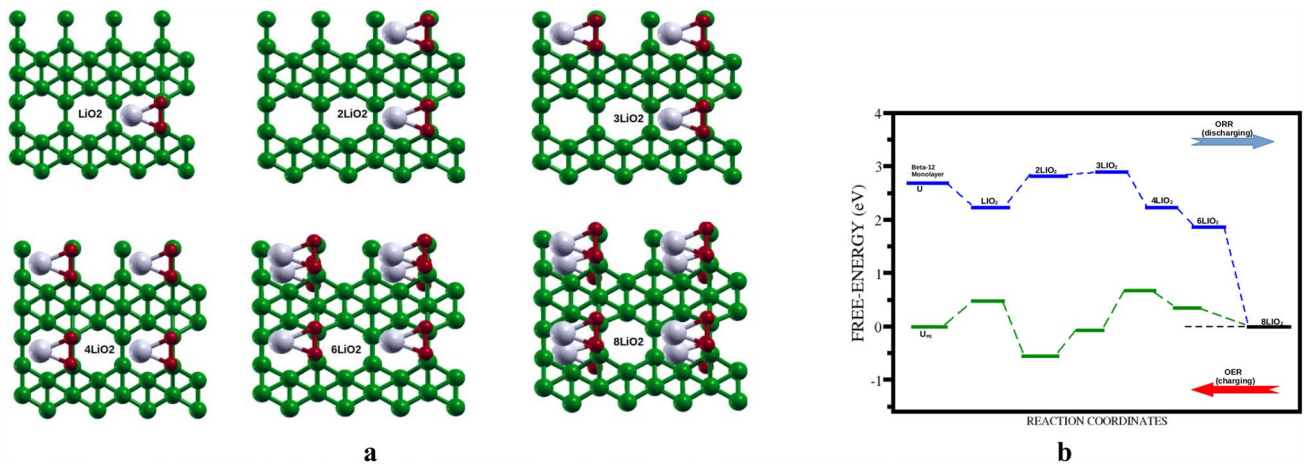

Fig. 8 **a** Increased concentration of the LiO_2 on β_{12}-borophene, and **b** Gibbs free energies in the ORR process

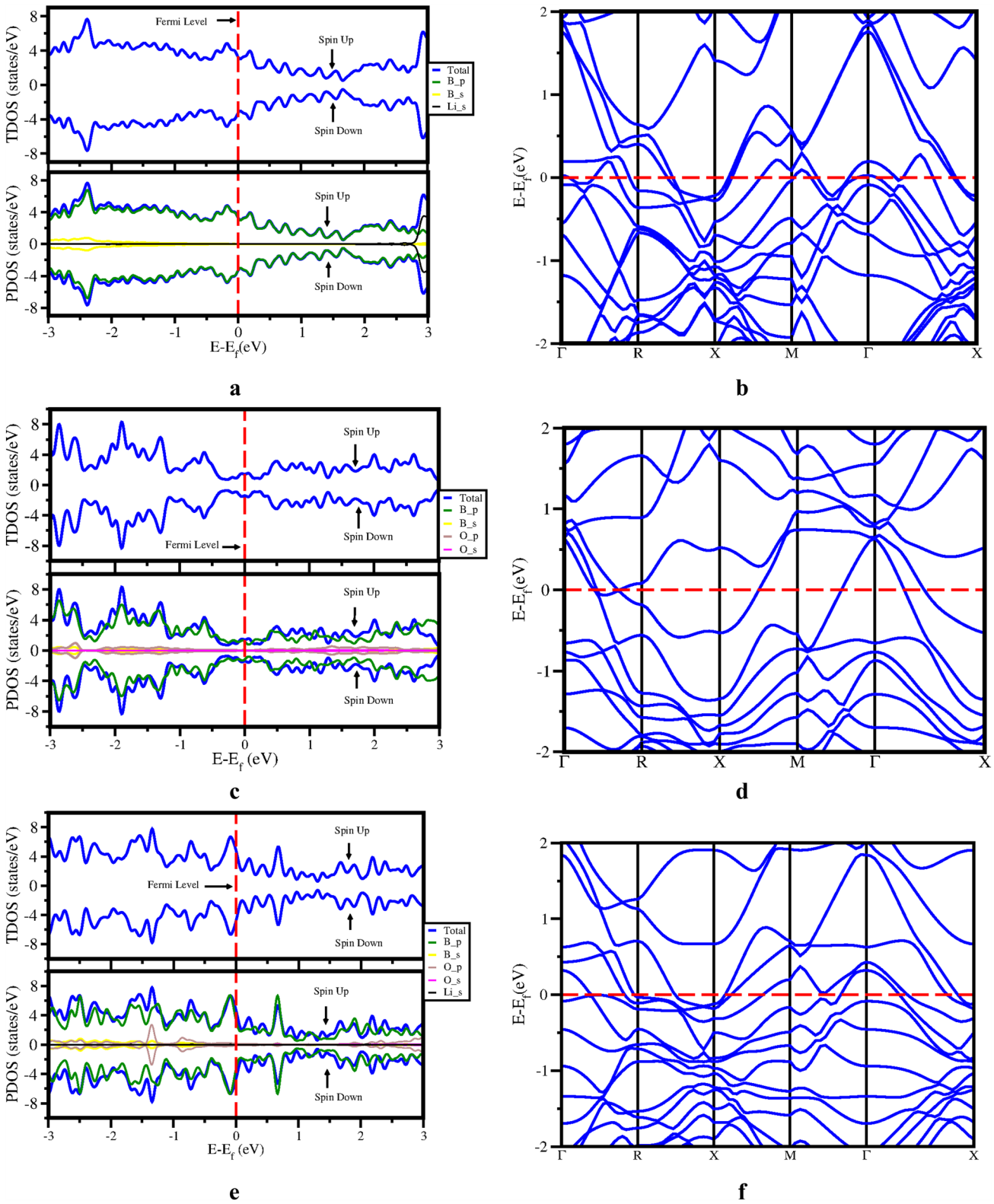

Fig. 9 Spin-orbitals density of states and bands structures: **a–b** Li on β_{12}-borophene, **c–d** O_2 on β_{12}-borophene, (**e–f**) LiO_2 on β_{12}-borophene. The Fermi level is set at zero mark and denoted by a dashed red line

the bridge with its axis parallel to boron atoms, with Li atom on top (SITE 2G), and (h) Li facing the bridge with O_2 on top and its axis parallel to the bridge (SITE 2H).

After relaxing the systems, the configurations maintained their positions and orientations. However, the binding distances for the configurations varied (Table 3). The binding distances were calculated by considering the distances between Li-substrate and O_2-substrate. The Li-substrate binding distances ranged from 1.55 to 5.21 Å, while the O_2-substrate distances ranged from 1.54 to 3.48 Å. Furthermore, the adsorption energies were calculated and ranged from − 3.70 to − 0.88 eV (Table 4). Among the configurations tested, the one at SITE 2D exhibited had shortest binding distance and the most negative adsorption energy, this is due to the covalent bonds formed between O_2 and boron (Fig. 6d). These results suggest that it is the most energetically stable configuration.

Topological and quantitative analysis of charge density difference distributions

Following the calculation of adsorption energies and identification of the most energetic configurations, a detailed understanding of the electronic interactions between the adsorbates and the substrate was gained by calculating the charge density difference distributions. This was followed by a comprehensive topological analysis of the charge iso-surfaces (Fig. 7). Furthermore, using the Bader analysis scheme (Tang et al. 2009; Henkelman et al. 2006), the charge was quantified and later compared to the adsorption energies. The results revealed that; for Li on β_{12}-borophene there was an accumulation of charge (yellow) towards the substrate from the lithium-ion (Fig. 7a). This demonstrates the low electronegativity of lithium-ion and its tendency to donate about 0.88 |e| to the substrate. The transferred electric charge confirms ionic bonding in the Li-substrate system. Then for O_2 on β_{12}-borophene (Fig. 7b), it was found that despite the formation of covalent bonds, charge depleted (blue) from the β_{12}-borophene and accumulated (yellow) towards O_2. This indicates the high electronegativity of oxygen, and because of the covalent bonds formed, a charge of 1.98 |e| was shared between the O_2 and the substrate. This significant quantified charge shared explains why O_2 has a big negative adsorption energy value. Finally, for LiO_2 on β_{12}-borophene (Fig. 7c), the charge distribution mechanism is complex. Initially, the charge is accumulated (yellow) by the substrate and depleted (blue) from the lithium atom, transferring a quantified charge of about 0.89 |e|. Then the charge is accumulated (yellow) towards O_2 and depleted (blue) from the β_{12}-borophene, sharing about 1.76 |e| due to covalent bond formation. Therefore, the total electronic charge transferred between lithium superoxide and the substrate is determined to be 0.86 |e|. When analyzing the adsorption energies of Li, O_2, and LiO_2 with their corresponding quantified charge densities (Table 4), it becomes evident why the adsorption energy values for Li (− 2.24 eV) and LiO_2 (− 3.70 eV) are smaller than for O_2 (− 5.15 eV).

Ultimately, from the analysis above it is very evident that the values of the adsorption energies correspond to the quantified charge densities transferred, showing that the larger the quantity of charge being transferred the more the adsorbate is being anchored onto the substrate. After comparing the binding distances and the quantified charges, it was found that for Li (2.00 Å) and LiO_2 (1.79 Å), the binding distances are longer than for O_2 (1.69 Å). Showing that the shorter the binding distance, the larger the quantity of charge being transferred. The values obtained suggest a strong electronic interaction between O_2 and the substrate.

Gibbs free energies and potential of the adsorbed LiO2 during ORRs mechanism

As earlier mentioned, in the $Li-O_2$ battery the mechanisms rely on the oxygen reduction reactions (ORRs). The proposed mechanism to form the LiO_2 as the intermediate discharge product at the surface of the cathode is as follows (Yang et al. 2018; Ji et al. 2017):

$$Li^+(s) + e^- + O_2(g) + \beta_{12}(s) \rightarrow LiO_2^*(s) \tag{6}$$

Here, LiO^* represents the complex system (LiO_2 adsorbed on the β_{12}-borophene). Therefore, to obtain the free energies, the following equation was used (Xu et al. 2018; Yang et al. 2018):

$$\begin{aligned}\Delta G(LiO_2^*) &= \Delta G(Li^+ + e^- + O_2 + \beta_{12} \rightarrow LiO_2^*) \\ &= CP_{LiO2^*} - CP_{Li} - CP_{O_2} - CP_{\beta 12}\end{aligned} \tag{7}$$

By employing the calculated values of the chemical potentials (Table 5) and Eq. 7, we derived the Gibbs free energies (Fig. 8b). Subsequently, using Eq. 4, the potentials were calculated and determined the overpotential (− 1.87 V) the complete reactions. The moderate value of overpotential obtained indicates that the formation of LiO_2 at the surface of the β_{12}-borophene is spontaneous.

Metallic characteristics for systems of species on β_{12}-borophene

After calculating the Gibbs free energy changes, the electronic transport characteristics were investigated for all the species involved in the reactions. This was achieved by calculating the density of states for the following systems: (i) Li on β_{12}-borophene, (ii) O_2 on β_{12}-borophene, and (iii) LiO_2 on β_{12}-borophene. These results were then compared with the electronic structures of pristine β_{12}-borophene (Fig. 2).

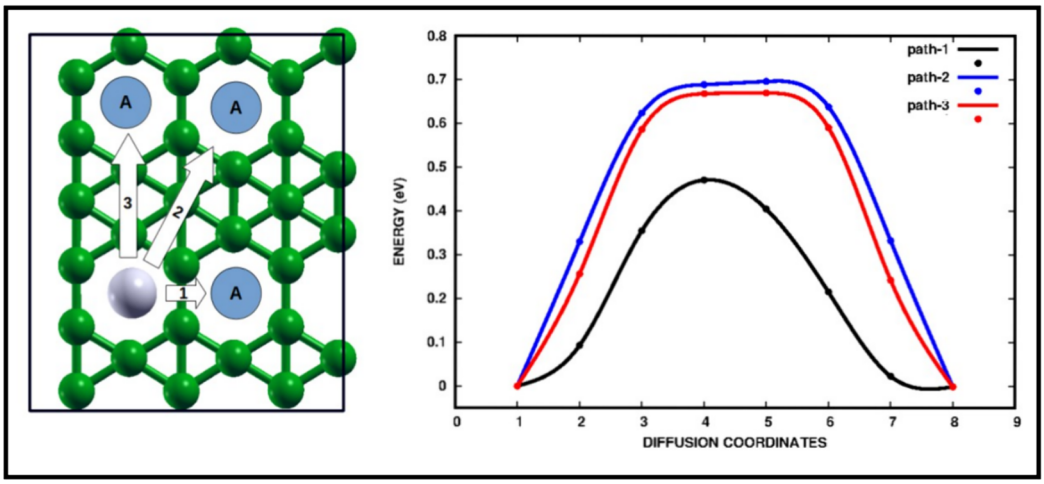
A
A
A
A
3
2
1
ENERGY (eV)
DIFFUSION COORDINATES
path-1
path-2
path-3

a

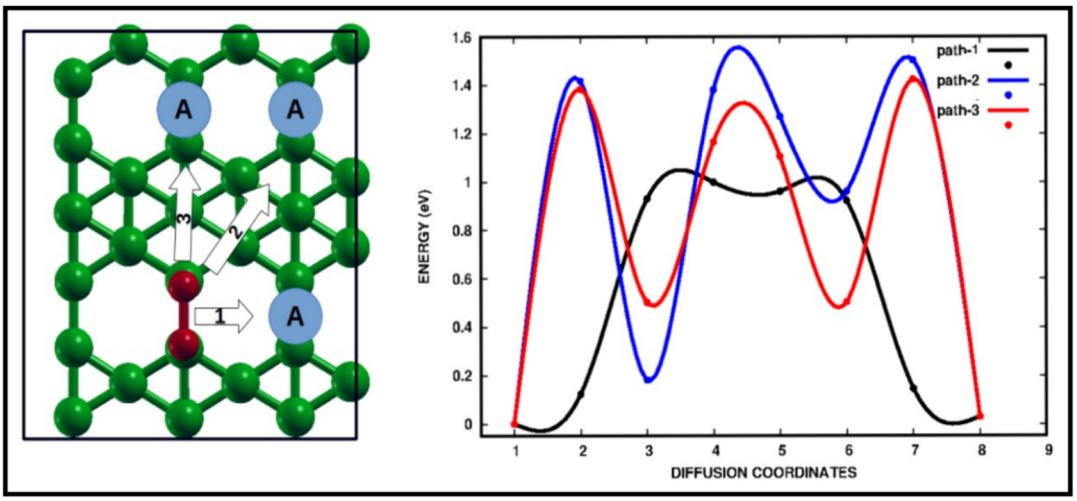
A
A
A
3
2
1
ENERGY (eV)
DIFFUSION COORDINATES
path-1
path-2
path-3

b

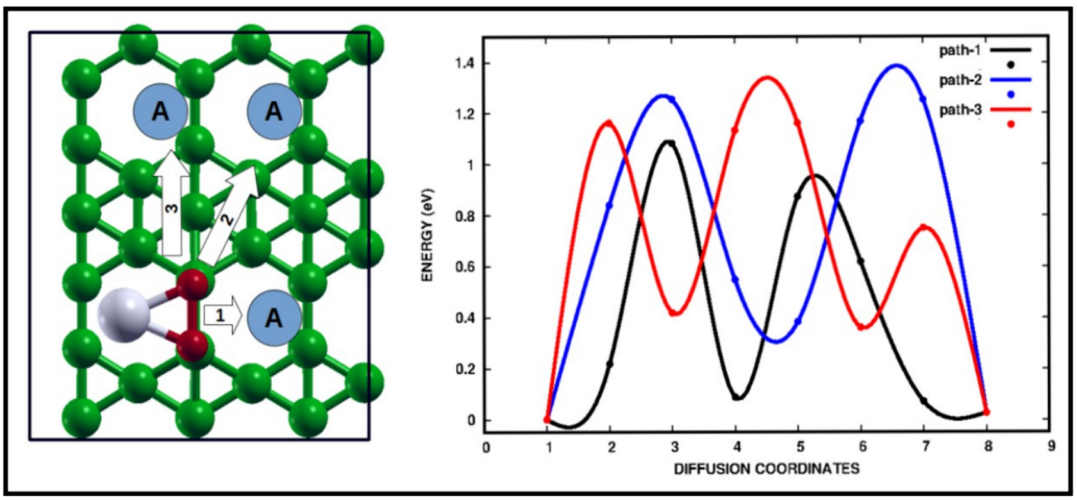
A
A
A
3
2
1
ENERGY (eV)
DIFFUSION COORDINATES
path-1
path-2
path-3

c

◂**Fig. 10** Top views of possible diffusion paths and energy profiles: **a** Li on β_{12}-borophene system and energy profile **b** O_2 on β_{12}-borophene system and energy profile, and **c** LiO_2 on β_{12}-borophene system and energy profile. The path-1, path-2, and path-3 on the diffusion energy profiles are represented by lines with black, red, and blue colors, respectively. All the adjacent stable sites on the crystal structure are denoted by A in a blue circle (around the hollow hexagons). The lithium, oxygen, and boron atoms are represented by the colors grey, red, and green, respectively

Table 6 Calculated diffusion energy barriers in different paths

Diffusion Energy Barrier (eV)			
System	path-1	path-2	path-3
Li on β_{12}	0.47	0.69	0.67
O_2 on β_{12}	0.91	1.55	1.42
LiO_2 on β_{12}	1.08	1.25	1.16

For Li on β_{12}-borophene (Fig. 9a, b), the Fermi level shifted upwards, and the bands moved downwards. This shift was attributed to the high tendency of lithium ions to donate electrons. Furthermore, the orbital levels along the Fermi level increased (Fig. 9a), suggesting easier drifting of the electrons between the valency and conduction bands. In terms of the projected density of states at the vicinity of the Fermi level, the 2p-orbitals of the boron atoms dominated, with minimal contribution from the 2 s-orbitals of the lithium atom. Despite the minimal orbital state contribution from the lithium atom, there was an electronic structural transformation (Fig. 9a). Next, for O_2 on β_{12}-borophene (Fig. 9c, d), a noticeable downward shift of the Fermi level towards the valence bands was observed, while the bands themselves moved upwards. This shift was attributed to the propensity of O_2 to accept electrons, resulting in unoccupied electronic states in the valence bands. The orbital levels along the Fermi level decreased significantly (Fig. 9d). The primary contributors to the local orbitals along the Fermi level were the boron atom's 2p-orbitals, with minimal contribution from the oxygen atom's 2p-orbitals. The hybridization of oxygen and boron atoms' orbitals (up and down) caused a significant transformation of electronic states along the Fermi level (Fig. 9c). Despite the drastic change in the electronic structure, the overlap of the valence and conduction bands indicated the preservation of metallic characteristics. Finally, for LiO_2 on β_{12}-borophene (Fig. 9e, f), an upward shift of the Fermi level was noted and a corresponding downward movement of the bands compared to O_2 on β_{12}-borophene (Fig. 9a, b). There was a significant increase in the electronic states along the Fermi level, leading to a change in the electronic structure of the system. The projected density of states along the Fermi level was predominantly influenced by the boron atom's 2p-orbitals, with minimal contributions from oxygen 2p-orbitals (Fig. 9e). It is noted that the increase in orbital levels along the Fermi level signifies enhanced conductivity, demonstrating that despite adsorbing the insulating LiO_2, the material maintained its metallic characteristics.

Diffusion energy barrier

The diffusion energy barrier of an electrode is a significant electronic property in determining the rate at which species (ions) diffuse between the electrodes during the charging and discharging processes. To evaluate this property, the nudged elastic band (NEB) scheme was used (Jónsson et al. 1998; Henkelman and Jónsson 2000).

Before calculating the diffusion energy barriers, potential diffusion paths based on unique symmetries and adjacent stable sites (Fig. 10) were identified in all the systems: Path-1 involves diffusion along the chain of hollow hexagons, Path-2 involves diagonal diffusion towards the adjacent chain of hollow hexagons, and Path-3 involves diffusing perpendicularly between chains of hollow hexagons. After the calculations, the results revealed that: for Li on β_{12}-borophene (Fig. 10a), the energy barriers for paths 1, 2, and 3 were 0.47, 0.69, and 0.67 eV, respectively (Table 6). Path-1 demonstrated the lowest value (0.47 eV), indicating low resistance in that direction. Hence, lithium ions are more likely to diffuse along the chains of hollow hexagons (Liu et al. 2018). For Path-2 and Path-3 energy barrier values were all higher than for Path-1, indicating higher resistance towards these diffusion paths. These values have been consistently reported in most of the previous research works (Liu et al. 2018; Zhang et al. 2016; Mortazavi et al. 2017), with values ranging between 0.4 and 0.7 eV. The minimal variations in the previously reported values and with our work are attributed to different calculation conditions. Thereafter for O_2 on β_{12}-borophene (Fig. 10b); paths 1, 2, and 3, energy barrier values were found to be 0.91 eV, 1.55 eV, and 1.42 eV, respectively (Table 6). The lowest energy barrier was along path-1, indicating a preference for O_2 to diffuse along the chains of hollow hexagons. In contrast, paths 2 and 3 exhibited higher diffusion energy barriers, suggesting more resistance to diffusion in those directions.

The reported high energy barriers against the O_2 are strongly correlated with the material's strong anchoring (-5.15 eV), indicating significant challenges for O_2 diffusion on the β_{12}-borophene. This suggests that the material could prevent O_2 from desorbing into the electrolyte and migrating to the negative electrode (anode) during the discharging process. Finally for LiO_2 on β_{12}-borophene (Fig. 10c),; energy barrier values for paths 1, 2, and 3 were found to be 1.08, 1.25, and 1.16 eV, respectively (Table 6). Notably, Path-1 had the lowest, followed by Path-3 then Path-2. The lowest energy barrier along Path-1 indicates low resistance, suggesting a preference for diffusion along the chain of hollow hexagons. Therefore, we generalized the diffusion energy

barrier for LiO_2 on β_{12}-borophene to be 1.08 eV. The results obtained are almost the same as the previously reported on lithium polysulfide diffusing on β_{12}-borophene surface, with the energy barrier values ranging between 1.13 to1.18 eV (Grixti et al. 2018). The minimal difference could be due to the nature of the adsorbate anchored, but ultimately the energy barriers are moderate. Showing the ability of the β_{12}-borophene to allow adsorbates to diffuse effortlessly (Fig. 10).

Most interestingly, all the species were observed to diffuse preferentially along a chain of hollow hexagons (path-1), primarily due to the relatively low diffusion energy barrier in that path. The diffusion energy barrier was found to exhibit anisotropic, due to different values in different directions. The moderate diffusion energy barriers indicate the potential which β_{12}-borophene has to enhance the kinetics of LiO_2 on the surface of the cathode electrode, thereby improving the rate of discharging and charging processes.

Conclusion

In conclusion, this study employed the first principles-based DFT calculations to investigate the adsorption and diffusion mechanisms of LiO_2 and its impact on the electronic properties of β_{12}-borophene as a cathode electrode. Our findings revealed several important insights, where the calculated adsorption energy of LiO_2 on β_{12}-borophene was found to be − 3.70 eV, suggesting a strong tendency for the species to remain bound to the material during the discharging process, which is conducive for achieving a high specific capacity and energy density. The dynamics in the charge density distributions between LiO_2 and the β_{12}-borophene substrate exhibited complex behavior, with O_2 accumulating most of the charge from boron and Li atoms. At the same time, β_{12}-borophene as a substrate also acquired a fraction of the charge from Li. This is significant as it shows how electrons are injected into the system and adsorbate–substrate electronic interactions. Furthermore, for the spontaneity reactions, Gibbs free energies were calculated to check the efficiency of oxygen reduction reactions at the surface of β_{12}-borophene, and an overpotential of − 1.87 V was found, this moderate value suggests its significant electrocatalytic effects on the formation of LiO_2. Most interestingly, after adsorbing the non-conductive LiO_2, β_{12}-borophene retained its metallic electronic structure. It showed increased electronic states along the Fermi level, suggesting an improved electrical conductivity. This is particularly important for improving the performance of $Li-O_2$-based batteries, especially considering the reported poor conductivity of cathode electrodes. Additionally, this material has a relatively low diffusion energy barrier of 1.08 eV, implying effortless movement of LiO_2 across the material. Therefore, an increase in the kinetics of the discharge products leads to high specific capacity and energy density of the battery. All in all, the predicted electronic properties make β_{12}-borophene a promising cathode electrode electrocatalyst material for improving the electrical conductivity and reaction kinetics in next-generation lithium-oxygen batteries. While our work is limited to the adsorption, diffusion mechanisms, and effects of LiO_2 on the electronic properties of β_{12}-borophene, we encourage future research to explore the impact of lithium peroxide (Li_2O_2) on β_{12}-borophene, including their corresponding Gibbs-free energy changes, because Li_2O_2 is also among the discharge products produced during the electrochemical processes. These findings will also contribute to the general understanding and conclusion of the practical application of β_{12}-borophene as an electrocatalyst in lithium-oxygen batteries.

Acknowledgements The research received financial support from the University of Pretoria's Department of Innovation and Research. We are also grateful to the Center for High-Performance Computing (CHPC) in Cape Town, South Africa, for providing computational resources for our project (Project Name: MATS1429). Furthermore, R.E.M. acknowledges the financial support from the National Institute for Theoretical and Computational Sciences (NTheCS).

Funding Open access funding provided by University of Pretoria.

Data availability Data will be made available on request.

Declarations

Conflict of interest There is no conflict of interest being declared by the authors.

References

Aurbach D, McCloskey BD, Nazar LF, Bruce PG (2016) Advances in understanding mechanisms underpinning lithium–air batteries. Nat Energy 1(9):1–11

Avouris P, Dimitrakopoulos C (2012) Graphene: synthesis and applications. Mater Today 15(3):86–97

Berckmans G, Messagie M, Smekens J, Omar N, Vanhaverbeke L, Van Mierlo J (2017) Cost projection of state of the art lithium-ion batteries for electric vehicles up to 2030. Energies 10(9):1314

Blöchl PE (1994) Proj Augment-Wave Method Phys Rev B 50(24):17953

Bruce PG, Freunberger SA, Hardwick LJ, Tarascon J-M (2012) Li–o_2 and li–s batteries with high energy storage. Nat Mater 11(1):19–29
Chadi DJ (1977) Special points for brillouin-zone integrations. Phys Rev B 16(4):1746
Choi W, Lahiri I, Seelaboyina R, Kang YS (2010) Synthesis of graphene and its applications: a review. Crit Rev Solid State Mater Sci 35(1):52–71
Chowdhury C, Datta A (2018) Doped boron nitride surfaces: potential metal free bifunctional catalysts for non-aqueous li–o_2 batteries. Phys Chem Chem Phys 20(24):16485–16492
Davoudiniya M, Mirabbaszadeh K (2021) Effects of strain and electric fields on the electronic transport properties of single-layer β_{12}-borophene nanoribbons. Phys Chem Chem Phys 23(34):18647–18658
Dong H, Ji Y, Hou T, Li Y (2018) Two-dimensional siligraphenes as cathode catalysts for nonaqueous lithium-oxygen batteries. Carbon 126:580–587
Ehrlich S, Moellmann J, Reckien W, Bredow T, Grimme S (2011) System-dependent dispersion coefficients for the dft-d3 treatment of adsorption processes on ionic surfaces. ChemPhysChem 12(17):3414–3420
Ernzerhof M, Scuseria GE (1999) Assessment of the perdew–burke–ernzerhof exchange-correlation functional. J Chem Phys 110(11):5029–5036
Feng B, Zhang J, Liu R-Y, Iimori T, Lian C, Li H, Chen L, Wu K, Meng S, Komori F et al (2016) Direct evidence of metallic bands in a monolayer boron sheet. Phys Rev B 94(4):041408
Feng B, Zhang J, Zhong Q, Li W, Li S, Li H, Cheng P, Meng S, Chen L, Wu K (2016b) Experimental realization of two-dimensional boron sheets. Nat Chem 8(6):563–568
Fwalo C, Kochaev A, Mapasha R (2024) Investigating the effectiveness of borophene on anchoring and influence on kinetics of sodium superoxide in sodium–oxygen batteries. J Energ Storage 84:110977
Geaney H, O'Dwyer C (2015) Electrochemical investigation of the role of mno2 nanorod catalysts in water containing an anhydrous electrolytes for li–o 2 battery applications. Phys Chem Chem Phys 17(10):6748–6759
Giannozzi P, Baroni S, Bonini N, Calandra M, Car R, Cavazzoni C, Ceresoli D, Chiarotti GL, Cococcioni M, Dabo I et al (2009) Quantum espresso: a modular and open-source software project for quantum simulations of materials. J Phys: Condens Matter 21(39):395502
Giannozzi P, Andreussi O, Brumme T, Bunau O, Nardelli MB, Calandra M, Car R, Cavazzoni C, Ceresoli D, Cococcioni M et al (2017) Advanced capabilities for materials modelling with quantum espresso. J Phys: Condens Matter 29(46):465901
Grimme S (2006) Semiempirical gga-type density functional constructed with a long-range dispersion correction. J Comput Chem 27(15):1787–1799
Grixti S, Mukherjee S, Singh CV (2018) Two-dimensional boron as an impressive lithium-sulphur battery cathode material. Energ Storage Mat 13:80–87
Halder A, Wang H-H, Lau KC, Assary RS, Lu J, Vajda S, Amine K, Curtiss LA (2018) Identification and implications of lithium superoxide in li–o2 batteries. ACS Energy Lett 3(5):1105–1109
He J, Ouyang Y, Yu C, Jiang P, Ren W, Chen J (2020) Lattice thermal conductivity of β_{12} and chi-3 borophene. Chin Phys B 29(12):126503
Henkelman G, Jónsson H (2000) Improved tangent estimate in the nudged elastic band method for finding minimum energy paths and saddle points. J Chem Phys 113(22):9978–9985
Henkelman G, Arnaldsson A, Jónsson H (2006) A fast and robust algorithm for bader decomposition of charge density. Comput Mater Sci 36(3):354–360
Hieu NN, Nguyen CV, Phuc HV, Hoi BD (2023) On the impact of adsorbed gas molecules on the anisotropic electro-optical properties of $\beta\beta_{12}$-borophene. Phys Chem Chem Phys 25(35):23829–23835
Hoi BD, Le TTP, Dung PV, Phong TC (2024) Substrate-induced strain and exchange field effects on the electronic and thermal properties of monolayer $\beta\beta_{12}$-borophene. Phys Chem Chem Phys 26(9):76511
Höök M, Tang X (2013) Depletion of fossil fuels and anthropogenic climate change—a review. Energy Policy 52:797–809
Jemmis ED, Jayasree EG (2003) Analogies between boron and carbon. Acc Chem Res 36(11):816–824
Ji Y, Dong H, Yang M, Hou T, Li Y (2017) Monolayer germanium monochalcogenides (ges/gese) as cathode catalysts in nonaqueous li–o 2 batteries. Phys Chem Chem Phys 19(31):20457–20462
Jiang H, Zhao T, Shi L, Tan P, An L (2016) First-principles study of nitrogen-, boron-doped graphene and co-doped graphene as the potential catalysts in nonaqueous li–o2 batteries. J Phys Chem C 120(12):6612–6618
Jiang H, Shyy W, Liu M, Ren Y, Zhao T (2018) Borophene and defective borophene as potential anchoring materials for lithium–sulfur batteries: a first-principles study. J Mat Chem A 6(5):2107–2114
Jónsson H, Mills G, Jacobsen KW (1998) Nudged elastic band method for finding minimum energy paths of transitions. Classical and quantum dynamics in condensed phase simulations. World Scientific, pp 385–404
Kamat PV (2019) Lithium-ion batteries and beyond: celebrating the 2019 nobel prize in chemistry–a virtual issue. ACS Energ Lett 4(11):2757–2759
Karimzadeh S, Safaei B, Jen T-C (2023) Investigation on electrochemical performance of striped, β β_{12} and chi-3 borophene as anode materials for lithium-ion batteries. J Mol Graph Model 120:108423
Li J-H, Yu Y-X (2021) Enhanced catalytic performance of pillared-mno_2 with enlarged layer spaces for lithium–and sodium–oxygen batteries: a theoretical investigation. Nanoscale 13(48):20637–20648
Li J-H, Yu Y-X (2021) How do oxygen vacancies influence the catalytic performance of two-dimensional nb_2o_5 in lithium-and sodium-oxygen batteries? Chemsuschem 14(24):5488–5498
Li D, Gao J, Cheng P, He J, Yin Y, Hu Y, Chen L, Cheng Y, Zhao J (2020a) 2d boron sheets: structure, growth, and electronic and thermal transport properties. Adv Func Mater 30(8):1904349
Li J-H, Wu J, Yu Y-X (2020b) Theoretical exploration of single-layer tl2o as a catalyst in lithium–oxygen battery cathodes. J Phys Chem C 124(17):9089–9098
Li JH, Wu J, Yu YX (2021) Singlet oxygen vs. triplet oxygen: functions of 2d-moo 3 catalysts in conquering catastrophic parasitic-reactions in lithium–and sodium–oxygen batteries. J Mat Chem A 9(16):10186–10198
Liu J, Zhang L, Xu L (2018) Theoretical prediction of borophene monolayer as anode materials for high-performance lithium-ion batteries. Ionics 24:1603–1615
Liu T, Vivek JP, Zhao EW, Lei J, Garcia-Araez N, Grey CP (2020) Current challenges and routes forward for nonaqueous lithium–air batteries. Chem Rev 120(14):6558–6625
Lu J, Jung Lee Y, Luo X, Chun Lau K, Asadi M, Wang H-H, Brombosz S, Wen J, Zhai D, Chen Z et al (2016) A lithium–oxygen battery based on lithium superoxide. Nature 529(7586):377–382
Luo Z, Fan X, An Y (2017) First-principles study on the stability and stm image of borophene. Nanoscale Res Lett 12:1–8
Mamun A-A, Liu Z, Rizzo DM, Onori S (2018) An integrated design and control optimization framework for hybrid military vehicle using lithium-ion battery and supercapacitor as energy storage

devices. IEEE Transactions on Transportation Electrification 5(1):239–251
Mannix AJ, Zhou X-F, Kiraly B, Wood JD, Alducin D, Myers BD, Liu X, Fisher BL, Santiago U, Guest JR et al (2015) Synthesis of borophenes: anisotropic, two-dimensional boron polymorphs. Science 350(6267):1513–1516
Marder MP (2010) Condensed matter physics. Wiley
Methfessel M, Paxton A (1989) High-precision sampling for brillouin-zone integration in metals. Phys Rev B 40(6):3616
Momma K, Izumi F (2008) Vesta: a three-dimensional visualization system for electronic and structural analysis. J Appl Crystallogr 41(3):653–658
Monkhorst HJ, Pack JD (1976) Special points for brillouin-zone integrations. Phys Rev B 13(12):5188
Mortazavi B, Rahaman O, Ahzi S, Rabczuk T (2017) Flat borophene films as anode materials for mg, na or li-ion batteries with ultra high capacities: a first-principles study. Appl Mater Today 8:60–67
Neugebauer J, Scheffler M (1992) Adsorbate-substrate and adsorbate-adsorbate interactions of na and k adlayers on al (111). Phys Rev B 46(24):16067
Peng B, Zhang H, Shao H, Ning Z, Xu Y, Ni G, Lu H, Zhang DW, Zhu H (2017) Stability and strength of atomically thin borophene from first principles calculations. Mat Res Lett 5(6):399–407
Perdew JP, Burke K, Ernzerhof M (1998) Perdew, burke, and ernzerhof reply. Phys Rev Lett 80(4):891
Placke T, Kloepsch R, Dühnen S, Winter M (2017) Lithium ion, lithium metal, and alternative rechargeable battery technologies: the odyssey for high energy density. J Solid State Electrochem 21:1939–1964
Rao D, Liu X, Yang H, Zhang L, Qiao G, Shen X, Xiaohong Y, Wang G, Lu R (2019) Interfacial competition between a borophene-based cathode and electrolyte for the multiple-sulfide immobilization of a lithium sulfur battery. J Mat Chem A 7(12):7092–7098
Rubab A, Baig N, Sher M, Sohail M (2020) Advances in ultrathin borophene materials. Chem Eng J 401:126109
Scerri E (2019) The periodic table: its story and its significance. Oxford University Press
Stampfl C, Mannstadt W, Asahi R, Freeman AJ (2001) Electronic structure and physical properties of early transition metal mononitrides: density-functional theory lda, gga, and screened-exchange lda flapw calculations. Phys Rev B 63(15):155106
Sun X, Liu X, Yin J, Yu J, Li Y, Hang Y, Zhou X, Yu M, Li J, Tai G et al (2017) Two-dimensional boron crystals: structural stability, tunable properties, fabrications and applications. Adv Func Mater 27(19):1603300
Tan P, Jiang H, Zhu X, An L, Jung C, Wu M, Shi L, Shyy W, Zhao T (2017) Advances and challenges in lithium-air batteries. Appl Energy 204:780–806
Tang W, Sanville E, Henkelman G (2009) A grid-based bader analysis algorithm without lattice bias. J Phys: Condens Matter 21(8):084204
Wieser ME, Coplen TB (2010) Atomic weights of the elements 2009 (iupac technical report). Pure Appl Chem 83(2):359–396
Xu H, Cheng D, Cao D, Zeng XC (2018) A universal principle for a rational design of single-atom electrocatalysts. Nat Catal 1(5):339–348
Yang Y, Wang Y, Yao M, Wang X, Huang H (2018) First-principles study of rocksalt early transition-metal carbides as potential catalysts for li–o 2 batteries. Phys Chem Chem Phys 20(48):30231–30238
Yu Y-X (2019) Effect of defects and solvents on silicene cathode of nonaqueous lithium–oxygen batteries: a theoretical investigation. J Phys Chem C 123(1):205–213
Yu X, Chen F, Yu Z, Li Y (2020) Computational study of borophene with line defects as sensors for nitrogen-containing gas molecules. ACS Appl Nano Mat 3(10):9961–9968
Zhang X, Hu J, Cheng Y, Yang HY, Yao Y, Yang SA (2016) Borophene as an extremely high capacity electrode material for li-ion and na-ion batteries. Nanoscale 8(33):15340–15347